Applied Thermal Engineering 224 (2023) 120123

Contents lists available at ScienceDirect

Applied Thermal Engineering

journal homepage: www.elsevier.com/locate/apthermeng

Research Paper

Thermo-economic optimization of a novel confined thermal energy storage system based on granular material

E. Cano-Pleite *, F. Hernández-Jiménez, L.M. García-Gutiérrez, A. Soria-Verdugo

Department of Thermal and Fluid Engineering, University Carlos III of Madrid, Av. Universidad 30, Leganés, Madrid, Spain

ARTICLE INFO

Keywords:
Exergy
Granular material
Optimization
Thermocline
TES

ABSTRACT

Concentrated solar power is a suitable technology for production of green electricity. However, to attain a uniform electricity production, concentrated solar power should be coupled with large Thermal Energy Storage (TES) systems. Among the different technologies of TES systems, storage of sensible heat in granular material is widely used due to its simple operation. These TES systems store energy as an increase of temperature of a large mass of small solid particles, through which a fluid circulates exchanging heat. TES systems are typically operated in a fixed bed regime, maximizing their exergy output, thus limiting the maximum allowable velocity of the fluid flow. In this work, a novel confined bed is proposed to mechanically prevent the motion of the solid particles conforming the TES system even for high fluid velocities, to guarantee that the exhaust temperature of the fluid is maximum during a discharge process. In this novel confined bed, a thermocline evolves from bottom to top of the system, separating the low and high temperature of the bed during the discharge process. An analytical model was applied to describe the evolution of the thermocline and the effect of the different operating parameters on the thermocline thickness.

The effect of the thermocline thickness was combined with a thermo-economic analysis of a confined bed TES system proposed for a case of study. The new confined bed here proposed was optimized considering thermodynamics aspects, namely the fluid exergy increment in the bed, and economic factors, specifically the total investment cost of the TES system. The optimization resulted in low values of the fluid velocity, between 0.2 and 0.4 m/s, but still higher than the minimum fluidization velocity of sand particles of 750 μm, justifying the requirement of a confined bed, and low bed aspect ratios, between 0.25 and 0.9, to prevent excessively high fluid pressure drops. However, the bed aspect ratio increases significantly for higher granular material particle sizes, up to a ratio of bed height to diameter of 3 for a particle size of 10 mm and a TES demand time of 6 h.

1. Introduction

The depletion of fossil fuels and the requirement of reducing the anthropogenic pollutant emissions to the atmosphere motivate the search of renewable technologies capable of supplying the increasing electric energy demand with limited or null associated emissions. In this sense, Concentrated Solar Power (CSP) plants are a suitable alternative to fossil fuels, especially in countries where solar irradiation is high. CSP plants commonly integrate large Thermal Energy Storage (TES) systems to produce electricity uniformly for several hours, even though solar irradiation is highly non-steady. TES systems can store energy in the central hours of the day, when solar irradiation is high, and release the stored energy later, once solar irradiation decreases, allowing the operation of the power block of the plant under steady state conditions. In addition, TES systems can also soften the short-term fluctuations of the energy captured by CSP plants caused by the transient blockage of solar irradiation incident in concentrators by passing clouds [10].

Three main technologies of TES systems are currently available: sensible heat storage, latent heat storage, and thermochemical heat storage [18]. Sensible heat storage consists in storing energy in the form of an increase of temperature in a substance, whereas latent heat storage system takes advantage of the phase change energy of the storage material. In contrast, energy is stored in thermochemical heat storage systems by means of a reversible chemical reaction, which is endothermal in one direction and exothermal in the opposite direction. Among the different alternatives for TES systems, sensible heat storage is the most mature, and thus, the most widely used technology for large scale [23]. The storage materials used in sensible heat storage systems can be liquids or solids. Among the liquids, molten salts are widely used

* Corresponding author.
E-mail address: edcanop@ing.uc3m.es (E. Cano-Pleite).

https://doi.org/10.1016/j.applthermaleng.2023.120123
Received 5 September 2022; Received in revised form 3 January 2023; Accepted 25 January 2023
Available online 31 January 2023

Nomenclature

A	Area [m^2]
Bi	Biot number [–]
c_p	Specific heat [J kg^{-1} K^{-1}]
C	Investment cost [$]
d_s	Solids diameter [m]
D	TES vessel diameter [m]
D^*	Dimensionless diffusion coefficient [–]
E	Exergy [W]
g	Gravity acceleration [m s^{-2}]
H	Height of the TES vessel [m]
i	Specific enthalpy [J kg^{-1}]
k	Thermal conductivity [W m^{-1} K^{-1}]
m_s	Mass of solid particles [kg]
$\dot{m}_f$	Fluid mass flow rate [kg s^{-1}]
Nu	Nusselt number [–]
Pe	Peclet number [–]
Pr	Prandtl number [–]
q_{loss}	Heat dissipated through TES walls [W]
p	Pressure [Pa]
r	Radial coordinate [m]
R	TES vessel radius [m]
Re	Reynolds number [–]
R_g	Individual gas constante of air [J kg^{-1} K^{-1}]
s	Specific entropy [J kg^{-1} K^{-1}]
t	time [s]
t_d	Discharge time [h]
t_i	TES demand time [h]
T	Temperature [K]
u	Fluid velocity [m s^{-1}]
u^*	Dimensionless fluid velocity [–]
U	Global heat transfer coefficient [W m^{-2} K^{-1}]
V	TES volume [m^3]
z	height coordinate [m]

Greek letters:

β	Dimensionless thermal conductivity [–]
γ	Dimensionless volumetric heat capacity [–]
δ_t	Thermocline thickness [m]
ε	Void fraction [–]
ζ	Dimensionless height [–]
η	Isentropic efficiency [–]
η_p	Politropic efficiency [–]
θ	Dimensionless temperature [–]
λ	Dimensionless thermocline thickness [–]
μ	Dynamic viscosity [kg m^{-1} s^{-1}]
π_p	Compressor pressure ratio [–]
ρ	Density [kg m^{-3}]
σ	Thermocline thickness deviation [–]
τ	Dimensionless time [–]
ϕ	Percentage of volume occupied [–]

Abbreviations:

CSP	Concentrated Solar Power
SM	Solar Multiples
TES	Thermal Storage System

Subscripts:

0	Dead state
a	Ambient
ct	center
c	Compressor
dist	Distributor
eff	Effective
ext	External wall
f	Fluid phase
fg	Foam glass
found	Foundations
h	High
in	Inlet
int	Intermediate
l	Low
mat	TES material
mc	Microporous
mf	Minimum fluidization
min	Minimum
out	Outlet
opt	Optimal
s	Solid phase, sand
ss	Stainless steel
t	Thermocline
w	Wall

to store sensible heat due to their favorable heat transfer properties [32]. However, the use of molten salt has also some drawbacks, such as the higher investment cost due to the usage of two storage tanks in most cases and the limited temperature operation, which should always be between the crystallization and the decomposition temperature of molten salts [7]. Regarding solids as basis material for sensible heat storage, a single tank filled with granular material can be used to reduce costs and the operating temperature can be increased up to 1000 °C, which is beneficial for the performance of the turbine to which the TES system outlet is connected [39]. Furthermore, the high temperature attainable by sensible heat TES systems using solids as storage material permits the use of working fluids such as air or supercritical CO_2 for which improved power cycles can be designed, leading to higher conversion efficiencies [6,30].

When a working fluid circulates through a bed of small solid particles in the upwards direction, the characteristics of the system depend strongly on the fluid velocity. For low fluid velocities, the fluid percolates through the voids between solid particles, which remain stationary, in what is called a fixed bed regime. At a certain value of the fluid velocity, the drag force of the fluid on the particles balances their gravity force. Then, the solid particles are suspended in the fluid, presenting a radical reduction of the friction between adjacent particles. This kind of bed is referred to as an incipiently fluidized bed and the fluid velocity is the so-called minimum fluidization velocity of the solid particles. The increase of the fluid velocity above the minimum fluidization velocity usually produces instabilities in the bed and the appearance of bubbles of fluid, in which is known as a bubbling fluidized bed [22]. The characteristics of fixed and bubbling fluidized beds differ remarkably. For instance, in terms of mixing, the stationary character of the solids in a fixed bed results in a null mixing of particles, whereas in bubbling fluidized beds, the motion of bubbles induces high degrees of solid mixing [34]. The high mixing of solids in bubbling fluidized beds leads to a homogeneous temperature of the entire bed during operation, which is one of the main advantages of bubbling fluidized bed reactors to hold chemical reactions in applications such as conversion of solid fuels, for which bubbling fluidized beds have higher conversion degrees than fixed beds [28].

For applications like energy storage as sensible heat in TES systems, the homogeneous temperature of bubbling fluidized beds is a significant drawback. While in a fixed bed reactor the discharge of the bed would be

progressive from bottom to top, presenting a thin thermocline that separates the zones of low and high temperature of the bed, the discharge under a bubbling fluidized bed regime will correspond to a uniform temperature reduction in the entire bed, following an inverse exponential decay of the bed temperature with time [17]. Therefore, from the point of view of the power block, connected to the outlet of the bed of solid particles conforming the TES system, the temperature of the fluid supplied to the turbine will be high during a long time if the bed is operated under a fixed bed regime, whereas an exponential reduction of the fluid temperature with time occurs when operating the bed under bubbling fluidized bed conditions. Therefore, the availability of exergy in the fluid supplied from the TES system to the power block will be maximized when operating the bed of granular material under a fixed bed regime, as stated by Hernández-Jiménez et al. [17]. Nevertheless, the operation of the TES system at fixed bed conditions requires a low velocity of the fluid, below the minimum fluidization velocity of the solid particles conforming the granular system, which may be a handicap for the application of these TES systems in large scale power plants, where the mass flow rate of fluid, and thus the velocity of fluid, are typically high. Considering these limitations, this work proposes as a novelty the use of a confined bed for the granular material TES system. In this novel system, the solid particles are mechanically confined between two gas distributors, one at the bottom and one at the top of the bed, preventing the appearance of bubbles, and thus the motion of particles, even for fluid velocities above the minimum fluidization velocity of the solids. Therefore, this new configuration using a confined bed operates as a fixed bed independently of the fluid velocity, showing the thermocline evolution and stratification of the bed, maximizing the exhaust temperature and exergy of the fluid at the outlet of the TES system during the discharge process.

The evolution of the thermocline in a granular material TES system can be characterized by solving the energy conservation equation of the solids and fluid. To that end, Votyakov and Bonanos [40] proposed a perturbation model to decouple the energy conservation equations. The model was later extended to account for the increase of the thermocline thickness as a function of time and location in the tank [2]. The analytical model of the thermocline evolution proposed by Votyakov and Bonanos [40] was originally validated with the results from Bayon and Rojas [4]. The model was further validated by the authors in Votyakov and Bonanos [41], Bonanos and Votyakov [2] and Bonanos and Votyakov [3] using numerical results of Yang and Garimella [45] and Hänchen et al. [16], and with experimental measurements of Meier et al. [26] and Hoffmann et al. [19]. This analytical model is valid provided that the solids conforming the granular material bed remain stationary. Thus, it will be valid both for fixed bed and for the proposed confined bed.

Different new storage bed concepts have been proposed to try to solve the main drawbacks of traditional cylindrical tanks, such as thermal ratcheting or high thermal losses, while other disadvantages arise. For example, Zanganeh et al. [46] proposed a truncated tank to reduce thermal ratcheting by guiding particles towards the upper part of the bed. This configuration increases the top surface through which the working fluid leaves the system at the highest temperature, therefore increasing its thermal losses. There are other more complex designs such as those proposed by Gauche [12] or Schlipf et al. [31] in which thermocline and flow instabilities appear. More recently, Trevisan et al. [38] proposed a novel radial flow packed bed TES system. The system presents limited pressure drops and thermal losses while the maximum thermal performance was 72 %. The thermal performance was penalized due to the appearance non-homogeneous temperature distribution at the outlet of the bed due to a non-uniform porosity distribution, which makes the thermocline evolution a critical aspect of the system. While these new designs present promising results, they also entail some drawbacks that make traditional cylindrical tanks worth to be enhanced and analyzed.

The number of works facing the optimization of sensible heat TES systems is relatively scarce. Marti et al. [25] performed a multi-objective optimization of a TES system based on different constrains. They considered two competing objectives: maximum exergy efficiency and minimal material costs, which were accounted for using the Pareto front. They applied the method to three pilot scale and an industrial scale unit, which allowed to select the most efficient design for a given cost or the cheapest design for a selected efficiency. Zhu et al. [47] carried out an optimization of the particle diameters in different layers of cascaded packed bed based on its exergy efficiency. Trevisan et al. [37] proposed novel quasi-dynamic boundary conditions to perform a techno-economic optimization of a packed bed TES system. The inlet design of a TES system based on molten salts was optimized to minimize the thermocline thickness by Weiss et al. [43]. Lou et al. [24] optimized the flow distribution in a molten salt TES system based on the thermocline evolution by introducing inlet and outlet manifolds. Other works studied combinedly the packed bed TES system with the power cycle in which it is integrated. In this sense, Trevisan et al. [36] developed a quasi-steady state thermo-economic model of the integrated concentrating solar power plant which includes the power cycle, the TES system, and the receiver. In general, the literature review suggests that the optimization of TES systems should be performed considering both thermodynamics and economic factors.

In this work an innovative granular material TES system is proposed based on a confined bed that mechanically prevents the fluidization of the solids conforming the bed to operate under a fixed bed regime at high fluid velocities. The stratified operation of the confined bed guarantees the supply of the fluid to the power block from the exhaust of the TES system with a maximum exergy availability for the complete discharge process. The novel confined bed TES system was optimized for the discharge of energy applied to a case of study in which the TES system is integrated in a CSP plant and coupled to an air Brayton cycle, using the operating parameters of Rovense et al. [30]. The discharging process (i.e., the TES system is already hot) is analyzed, since it is the most important process for the correct operation of the power block. However, an inverse similar analysis could be done for the charging process. The optimization of the confined bed was performed considering thermodynamic and economic aspects, by minimizing the total investment cost of the TES system per unit of fluid exergy increase.

2. Theory

2.1. Thermocline evolution

Granular material TES systems are composed of a large bed of small particles through which a fluid percolates. This TES systems store energy in the form of sensible heat by heating the solids at high temperature when an excess of heat is produced in the CSP plant and releasing that heat to the fluid once the thermal power required by the turbine cannot be reached by the solar system. When a fluid, with a different temperature, percolates through a bed of granular material where the solids remain stationary, a temperature front evolves from the inlet of the fluid, typically at the bottom of the bed, to the outlet of the fluid, commonly at the top of the bed. This temperature front, which separates the high and low temperature regions of the bed as shown in Fig. 1, is the so-called thermocline, whose thickness and location in the TES system depend on the operating conditions.

The evolution of the thermocline of a granular material TES system can be estimated from the temperature distribution of solids and fluid inside the packed bed. These temperature distributions can be determined analytically assuming one-dimensional plug flow for the fluid, no heat losses, and average uniform thermophysical properties for the solids and the fluid. Under these assumptions, the energy conservation equations for both the fluid and the solids in dimensionless form are, respectively [40]:

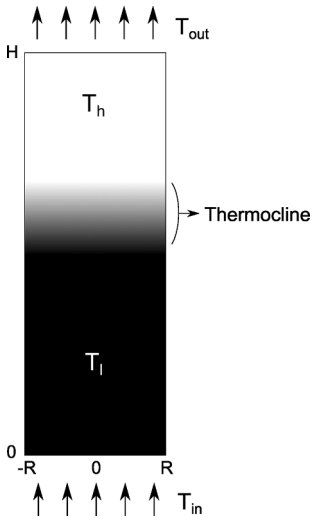

Fig. 1. Schematic view of the thermocline of a granular material TES system.

$$\gamma_f\left(\frac{\partial\theta_f}{\partial\tau}+\mathrm{Pe}\frac{\partial\theta_f}{\partial\zeta}\right)=\beta_f\frac{\partial^2\theta_f}{\partial\zeta^2}+\mathrm{Bi}\left(\theta_s-\theta_f\right) \tag{1}$$

$$\gamma_s\frac{\partial\theta_s}{\partial\tau}=\beta_s\frac{\partial^2\theta_s}{\partial\zeta^2}-\mathrm{Bi}\left(\theta_s-\theta_f\right). \tag{2}$$

The dimensionless temperatures for the fluid (f) and the solids (s) are determined as a function of the low, T_l, and high, T_h, temperatures of the TES system (notice that subscript i represents either the fluid f or the solids s):

$$\theta_i=\frac{T_i-T_l}{T_h-T_l}, \tag{3}$$

The dimensionless parameters for height, z, and time, t, in the energy conservation equations are determined as follows:

$$\zeta=\frac{z}{H} \tag{4}$$

$$\tau=\frac{t}{H^2}\frac{k_{eff}}{\left(\rho c_p\right)_{eff}}, \tag{5}$$

where the effective properties are calculated as a function of the properties of fluid (f) and solids (s), considering the void fraction, ε, as $X_{eff}=\varepsilon X_f+(1-\varepsilon)X_s$. The dimensionless form of the thermal conductivity, k_i, and volumetric heat capacity $\left(\rho c_p\right)_i$, for the fluid (f) and solids (s) are computed as follows:

$$\beta_i=\phi_i\frac{k_i}{k_{eff}} \tag{6}$$

$$\gamma_i=\phi_i\frac{\left(\rho c_p\right)_i}{\left(\rho c_p\right)_{eff}}, \tag{7}$$

where ϕ_i denotes the percentage of volume occupied by fluid (f) or solid (s), i.e., $\phi_f=\varepsilon$ and $\phi_s=1-\varepsilon$.

The remaining two factors affecting the energy conservation equations are the dimensionless numbers of Biot, Bi, and Pecklet, Pe, defined as follows:

$$\mathrm{Bi}=\frac{6(1-\varepsilon)k_f\mathrm{Nu}H^2}{k_{eff}{d_s}^2} \tag{8}$$

$$\mathrm{Pe}=\frac{uH\left(\rho c_p\right)_{eff}}{\varepsilon k_{eff}}. \tag{9}$$

where u is the velocity of the working fluid and d_s is the diameter of the granular material.

The heat transfer between the fluid and the solids is characterized by the Nusselt number, Nu, which can be estimated for a packed bed of granular material as a function of the Reynolds, Re, and Prandtl, Pr, numbers using the correlation of Wakao et al. [42]:

$$\mathrm{Nu}=\frac{hd_s}{k_f}=2+1.1\mathrm{Pr}^{\frac{1}{3}}\mathrm{Re}^{0.6} \tag{10}$$

where the common definitions of the Reynolds, and Prandtl, numbers are applied:

$$\mathrm{Re}=\frac{\rho_f u d_s}{\mu_f} \tag{11}$$

$$\mathrm{Pr}=\frac{\mu_f c_{pf}}{k_f}. \tag{12}$$

Votyakov and Bonanos [40] proposed a perturbation model to analytically solve the energy conservation equations for the fluid and the solids, Eqs. (1) and (2), which is founded on the assumption of a small difference between the fluid and the solids temperature, i.e., a low value of $\theta_s-\theta_f$, which is a reasonable assumption considering the high values of the convective coefficients found for fluids percolating though a fixed bed of granular material [11]. With the perturbation model of Votyakov and Bonanos [40], the energy conservation equations for the fluid and the solids, Eqs. (1) and (2), can be decoupled and transformed into:

$$\frac{\partial\theta_f}{\partial\tau}+u^*\frac{\partial\theta_f}{\partial\zeta}=D^*\frac{\partial^2\theta_f}{\partial\zeta^2} \tag{13}$$

$$\theta_s=\theta_f+\frac{\gamma_f\gamma_s\mathrm{Pe}}{\mathrm{Bi}}\frac{\partial\theta_f}{\partial\zeta}. \tag{14}$$

The parameters u^* and D^* in Eq. (13) are the dimensionless fluid velocity and diffusion coefficient, respectively, defined as follows:

$$u^*=\gamma_f\mathrm{Pe} \tag{15}$$

$$D^*=1+\frac{\left(\gamma_f\gamma_s\mathrm{Pe}\right)^2}{\mathrm{Bi}}. \tag{16}$$

The analytical solution of the perturbation model represented by Eqs. (13) and (14) is [40]:

$$\theta_f(\tau,\zeta)=\frac{1}{2}\left[1\pm erf\left(\frac{\zeta-u^*\tau}{\sqrt{4D^*\tau}}\right)\right] \tag{17}$$

$$\theta_s(\tau,\zeta)=\theta_f\pm\frac{\gamma_f\gamma_s Pe}{Bi}\frac{exp\left(-\frac{(\zeta-u^*\tau)^2}{4D^*\tau}\right)}{\sqrt{4\pi D^*\tau}}, \tag{18}$$

where the + sign applies for a discharge process and the - sign for a charge process, and erf represents the error function. According to Bell [1], the error function can be approximated with a precision higher than $3{\cdot}10^{-3}$ by the following exponential expression:

$$\mathrm{erf}(x)=\mathrm{sign}(x)\left[1-\exp\left(-\frac{4x^2}{\pi}\right)\right]^{\frac{1}{2}}. \tag{19}$$

Introducing the approximation of the error function, Eq. (19), in Eq. (17), the following expression for the dimensionless temperature of the fluid is derived:

$$\theta_f(\tau,\zeta)=\frac{1}{2}\left\{1\pm\mathrm{sign}(\zeta-u^*\tau)\left[1-\exp\left(-\frac{(\zeta-u^*\tau)^2}{\pi D^*\tau}\right)\right]^{1/2}\right\} \tag{20}$$

Eq. (20) can be rewritten in terms of the dimensionless center, ζ_{ct}, and thickness, λ, of the thermocline, which are defined as follows [41]:

$$\zeta_{ct}(\tau) = u^{*}\tau \tag{21}$$

$$\lambda(\tau) = \sqrt{4\pi D^{*}\tau}. \tag{22}$$

The parabolic rate law obtained for the dimensionless thickness of the thermocline is typical of a diffusion-controlled growth [35]. Introducing the expression for the center, ζ_{ct}, and thickness, λ, of the thermocline in Eq. (20), the dimensionless temperature of the fluid yields:

$$\theta_f(\tau,\zeta) = \frac{1}{2}\left\{1 \pm sign(\zeta-\zeta_{ct})\left[1-exp\left(-\left(\frac{\zeta-\zeta_{ct}}{\frac{\lambda}{2}}\right)^{2}\right)\right]^{\frac{1}{2}}\right\}. \tag{23}$$

According to Eq. (23), the temperature of the fluid changes from the low to the high temperature, i.e., θ_f changes from 0 to 1, when the distance to the center of the thermocline is below half of its thickness, that is, when $|\zeta - \zeta_{ct}| \leq \lambda/2$. The location of the center of the thermocline can then be determined as a function of time considering the height of the TES system, H, and ζ_{ct}:

$$z_t(t) = \zeta_{ct}H \tag{24}$$

The time evolution of the location of the center of the thermocline calculated by Eq. (24) obviously coincides with the evolution of the center of the thermocline location obtained from a global energy balance between the fluid and the solids:

$$z_t(t) = \frac{(\rho c_p)_f}{(\rho c_p)_{eff}}ut \tag{25}$$

The thermocline can also be defined as the region where θ_f varies from 0 to 1 to some extent σ, for instance, for a deviation of 5 %, $\sigma = 0.05$, from the low and high temperatures. In that case, the dimensionless thickness of the thermocline can be computed as follows:

$$\lambda_\sigma = \sqrt{4\pi D^{*}\tau log\frac{1}{4\sigma-4\sigma^{2}}}. \tag{26}$$

Therefore, the thickness of the thermocline can be determined, as a function of time, considering the height of the TES system of granular material:

$$\delta_t(t) = \lambda_\sigma H. \tag{27}$$

2.2. Exergy balance

During a discharge process, the fluid outlet of the granular material TES system is coupled to the turbine of the power cycle, for whose operation the exergy of the fluid flow is critical. Therefore, the discharge process, i.e., starting with the TES system at the high temperature and heating the fluid flow rate from the low to the high temperature, is set as the optimizing problem due to its strong effect of the performance of the power block of the plant. However, an inverse similar analysis could be done for the charge process.

The exergy balance for the fluid on the control volume enclosing the TES system (see the schematic in Fig. 1) is:

$$\Delta E = \dot{m}_f(\Delta i - T_0\Delta s) - \left(1-\frac{T_0}{T_w}\right)q_{loss}, \tag{28}$$

where ΔE is the exergy increment of the fluid, $\dot{m}_f$ is the mass fluid flow rate, Δi is its enthalpy variation between the inlet and the outlet, Δs is its entropy variation between the inlet and outlet, q_{loss} is the heat dissipated through the TES system walls, T_w is the temperature of the TES system interior wall, and T_0 is the reference temperature or temperature of the dead state, which is considered equal to the ambient temperature, T_a. The heat losses can be determined for each external surface of the TES system as follows:

$$q_{loss} = U_{ext}A_{ext}(T_w - T_a) \tag{29}$$

with U_{ext} being the global heat transfer coefficient through the external walls of the TES system, A_{ext} the external surface of TES system, T_w the TES system interior wall temperature, which will be the high or low temperature of the system depending on time and location in the bed. For the calculation of the heat losses through the TES system wall, the height of the system with a wall temperature equal to the low temperature is that below the center of the thermocline, calculated either by Eq. (24) or by Eq. (25), i.e., $T_w = T_l \Leftrightarrow z \leq z_t$, whereas the wall temperature above the center of the thermocline will be at the high temperature, i.e., $T_w = T_h \Leftrightarrow z > z_t$. The bottom and top wall temperatures are considered to be at the low and high temperatures, respectively, during the discharge process.

The required natural convection coefficients for the calculation of the global heat transfer coefficients U_{ext} were estimated using the classical correlations for free convection [20]. The TES system is considered insulated by three layers of different materials: stainless steel, microporous insulation, and foam glass. The thickness of each insulation layer was implemented as a function of the TES vessel diameter, D (see Table 1). The estimation of the thickness of the different insulation layers was made based on the thickness found in a literature review of TES systems [8,25]. These insulation materials and thicknesses ensure that the energy losses along a whole day are below 2 % of the thermal energy stored in the TES system.

The variation of enthalpy, Δi, and entropy, Δs, of the fluid required for the exergy balance, Eq. (28), can be determined from the ideal gas law, assuming the fluid as an ideal gas:

$$\Delta i = c_{p_f}(T_{out} - T_{in}), \tag{30}$$

$$\Delta s = c_{p_f}\log\frac{T_{out}}{T_{in}} - R_g\log\frac{p_{in}}{p_{in}+\Delta p}. \tag{31}$$

where c_{p_f} is the specific heat at constant pressure of the ideal gas, R_g is the individual gas constant of air, p_{in} is the inlet pressure of the fluid to the turbine, and Δp is the pressure drop of the fluid circulating through the confined bed TES system. There are two contributions for the fluid pressure drop: i) the pressure drop caused by the gas percolating through the packed bed of solid particles conforming the TES system, Δp_{bed}, and ii) the pressure drop due to the fluid distributors, Δp_{dist}, which should be high enough to guarantee a proper fluid distribution in the radial direction:

$$\Delta p = \Delta p_{bed} + \Delta p_{dist}. \tag{32}$$

The pressure drop of the gas percolating through a packed bed of solids, Δp_{bed}, can be calculated using Ergun's equation [9] and the pressure drop of the gas flowing across the distributor, Δp_{dist}, can be estimated using the classical recommendation from Karry and Werther [21] of setting the pressure drop of the distributor at 30 % of the pressure generated by the weight of the particles at minimum fluidization conditions, u_{mf}. This common value used for fluidized beds would ensure an even more uniform distribution of the flow in the cross section confined bed, given the higher pressure drop of the gas across the bed in the confined bed operation regime. Note that two distributors are used in this work, one at the bottom and another on top of the bed to mechanically prevent the movement of the solids, avoiding their fluidization during the discharging process. Also, the distributor situated at the

Table 1
TES vessel insulation layers and characteristics.

Insulation layer	Thickness	Thermal conductivity [W/mK]
Stainless steel	0.015D	20
Microporous	0.025D	0.025
Foam glass	0.025D	0.05

top part of the bed guarantees a proper distribution of the gas flow in the bed in case it is injected from its top part during the charging process, ensuring that the flow field inside the bed is uniform and retaining in this manner the thermal stratification of the system. The pressure drop of the bed and the distributors can be thus expressed as follows:

$$\Delta p_{bed} = u\left(\frac{150\mu_f H}{d_s^2}\frac{(1-\varepsilon)^2}{\varepsilon^3}\right) + u^2\left(\frac{1.75H\rho_f}{d_s}\frac{(1-\varepsilon)}{\varepsilon^3}\right), \tag{33}$$

$$\Delta p_{dist} = 0.6gH\rho_s(1-\varepsilon)\left(\frac{u}{u_{mf}}\right)^2, \tag{34}$$

where u is the velocity of the working fluid, ρ_f and μ_f are the density and dynamic viscosity of the fluid, respectively, H is the height of the bed, d_s is the particle side of the solids conforming the TES system, ε is the porosity of the bed, and g is the gravity acceleration.

2.3. Discharge time

There are several definitions of the discharge time of a granular material TES system depending on the objective of this parameter. The most widely used definition for the discharge time is the time required by the center of the thermocline, z_t, to attain the height of the TES system vessel, H. Using this definition, an expression of the discharge time, t_d, can be obtained by substituting z_t by H in Eq. (25) and isolating the time:

$$t_d = \frac{H}{u}\frac{(\rho c_p)_{eff}}{(\rho c_p)_f} \tag{35}$$

However, at $t = t_d$, the temperature of the fluid at the outlet of the TES system will be the average temperature between the high and the low temperature of the system. Thus, the exergy of the fluid at the exhaust of the TES system at that time would be substantially lower than that obtained when the fluid exits the TES system at the high temperature. Therefore, a better definition of the discharge time, in terms of the exergy availability of the fluid at the outlet of the TES system is the time required by the front of the thermocline to reach the TES vessel height, i.e., the time at which $z_t + \lambda_\sigma/2 = H$. This new definition of the discharge time results in more restricted times, guaranteeing that the exergy of the fluid leaving the TES system is still high to be converted in the power block. The discharge time to maximize the fluid exergy at the outlet of the TES system can be obtained from the following equation:

$$H = \frac{(\rho c_p)_f}{(\rho c_p)_{eff}} u t_d + \sqrt{\frac{\pi D^*}{H^2}\frac{k_{eff}}{(\rho c_p)_{eff}} log\frac{1}{4\sigma - 4\sigma^2} t_d} \tag{36}$$

The discharge time, defined as the time required by the front of the thermocline to reach the TES vessel height, can be obtained by solving Eq. (36) using a changing of variables, in the form $\xi^2 = t_d$, and solving the resulting quadratic equation. This definition of the discharge time will be used in this work to keep a maximum fluid exergy at the outlet of the TES system for the complete discharge process.

2.4. Thermo-economic optimization of the TES system

The exergy analysis can be combined with a cost analysis for a thermo-economic optimization of the TES system. For that purpose, all the costs involved in the manufacturing of the system should be considered. The total investment cost, C, is calculated as the summation of the cost of the TES system, C_{TES}, and the extra cost due to the requirement of a more powerful compressor, C_c, capable of overcoming the pressure drop generated by the fluid circulating through the TES system:

$$C = C_{TES} + C_c. \tag{37}$$

The cost of the TES system includes the cost of each of its components, namely, the TES granular material, the vessel of stainless steel, insulation layers composed of microporous insulation, and foam glass, and the foundation required to install the TES system. The specific cost, per unit of volume or area, of the TES system components, summarized in Table 2, were obtained from Marti et al. [25] and Trevisan et al. [36]. Note that each specific cost should be multiplied by its corresponding volume or area.

$$C_{TES} = C_{mat} + C_{ss} + C_{mp} + C_{fg} + C_{found}. \tag{38}$$

An estimation of the investment cost of a typical power cycle compressor working with dry air can be found in Ghaebi et al. [13]. This cost is a function of the compressor pressure ratio, the dry air mass flow rate, $\dot{m}_f$, and the efficiency of the compressor, η_c. Thus, the overrun due to the extra power required for the compressor to overcome the fluid pressure drop, Δp, can be estimated in US dollars as follows:

$$C_c = 71.1\frac{\dot{m}_f}{0.92 - \eta_c}\left[\frac{p_{in}}{p_a}\log\left(\frac{p_{in}+\Delta p}{p_{in}}\right) + \frac{\Delta p}{p_a}\log\left(\frac{p_{in}+\Delta p}{p_a}\right)\right] \tag{39}$$

where p_a is the ambient pressure.

Considering the exergy increment of the fluid in the TES system, ΔE, obtained from Eq. (28), and the total investment cost, C, estimated by Eq. (37), a thermo-economic optimization of the TES system can be carried out by minimizing the total investment cost per unit of exergy increment of the fluid, i.e., $C/\Delta E$, or by maximizing the exergy increment of the fluid per unit of cost, i.e., $\Delta E/C$.

3. Confined bed

In the novel confined bed TES system proposed in this work, two fluid distributors, at the bottom and the top of the bed, mechanically confine the granular material, preventing the fluidization of the solids and the appearance of bubbles even for fluid velocities above the minimum fluidization velocity of the solid particles. The fixed bed regime can be maintained in the confined bed TES system even for high fluid velocities, guaranteeing the operation of the single storage tank under stratified conditions both for the charging and discharging processes, with a thermocline separating the low temperature of the TES system located at the bottom and the high temperature of the system at the top. The thermocline evolves from bottom to top of the bed during a discharge process, increasing in thickness as described in Section 2. Thus, the confined bed allows a higher fluid exergy increment in the TES system maintained for long discharge times even for high values of the fluid velocity.

A schematic view of the confined bed TES system as a part of the CSP plant is depicted in Fig. 2. The concentrated solar power is used to heat air, which is the working fluid of the power block. When the solar thermal power received is higher than the power required for the nominal operation of the power block, the thermal power excess is charged in the TES system as sensible heat. For that, air is introduced through the top part of the granular bed that conforms the TES and leaves the system at a lower temperature through its bottom part, promoting a stratification of the system in a higher temperature region at the top part of the bed and a low temperature region at the bottom region. These two regions are separated by the thermocline. When the

Table 2
Specific costs of the TES system obtained from Marti et al. [25] and Trevisan et al. [36].

Specific cost	Value	Unit
TES material (mat)	66	[$/m^3]
Stainless steel (ss)	42,354	[$/m^3]
Microporous (mc)	4269	[$/m^3]
Foam glass (fg)	616	[$/m^3]
Foundations (found)	1210	[$/m^2]

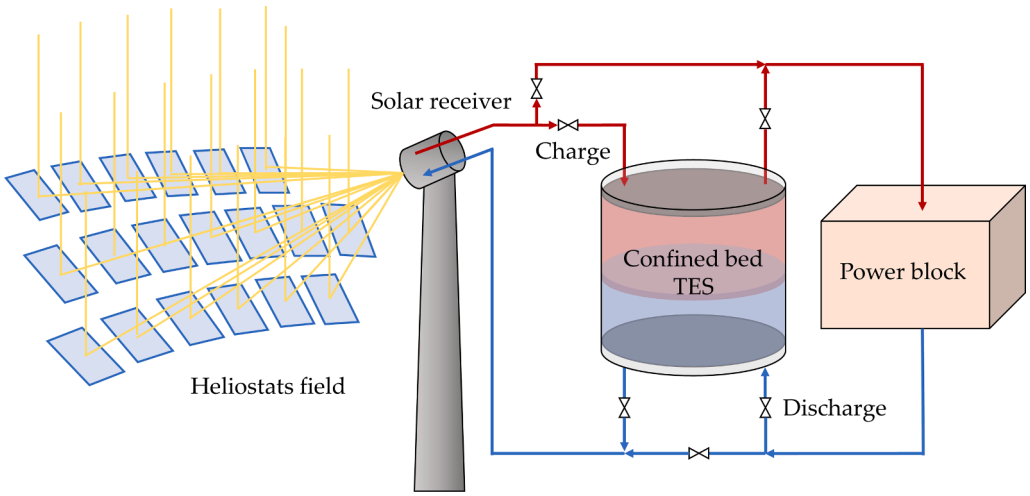

Fig. 2. Schematic view of the CSP plant using a granular material TES system.

thermal power concentrated in the central receiver is insufficient to operate the power block, the thermal energy previously stored in the TES system can be discharged introducing air through the bottom part of the bed, which exits the top part of the bed at a high temperature suitable for power generation in the power block. For simplicity, no air purification measures are included in the diagram shown in Fig. 2 nor considered in this work, as it is devoted to the study of the confined TES system. However, the appropriate measures shall be taken to ensure that no fine particles from the TES system are dragged through the turbine of the power block.

A schematic of the fixed bed, bubbling fluidized bed and confined bed operation as granular material TES system is depicted in Fig. 3. As discussed above, the fixed bed shows the separated zones of high T_h and low T_l temperature, while the bubbling fluidized bed operates at an intermediate temperature T_{int}, between the high and low values. However, the fluid velocity, and the corresponding mass flow rate, is limited in the case of the fixed bed to prevent fluidization by keeping the fluid velocity below the minimum fluidization velocity of the solid particles conforming the TES system. This limitation is solved by the proposed confined bed, which allows the operation of the bed with separated zones of high and low temperature and the evolution of a thermocline regardless of the fluid velocity. This results in a high mass flow rate of fluid at the outlet of the TES system at high temperature, i.e., a high mass flow rate of fluid with a high exergy availability, which is optimal for the power block coupled to the TES system.

4. Case of study

The thermo-economic procedure described in Section 2 was applied to optimize a granular material TES system for the plant proposed in Rovense et al. [30]. They modelled a closed Brayton cycle with intercooling coupled to a CSP plant in which the TES system is based on sensible heat storage. They proposed the analysis of two solar multiples, *SM*, of 1.5 and 2, and found that for $SM = 2$ the demand of hours fully covered by the TES system is 1, 5 and 12 h for the 21st of December, the 21st of March, and the 21st of June, respectively. Therefore, the TES system will be optimized for a range of demand hours from 1 to 12 h.

The TES system proposed by Rovense et al. [30] is a fluidized bed heat exchanger where the working fluid of the cycle flows inside tubes immersed in the fluidized bed. The particles conforming the bed were heated up with the working fluid when the solar availability was sufficient, during a charge process, and then they were stored in two tanks.

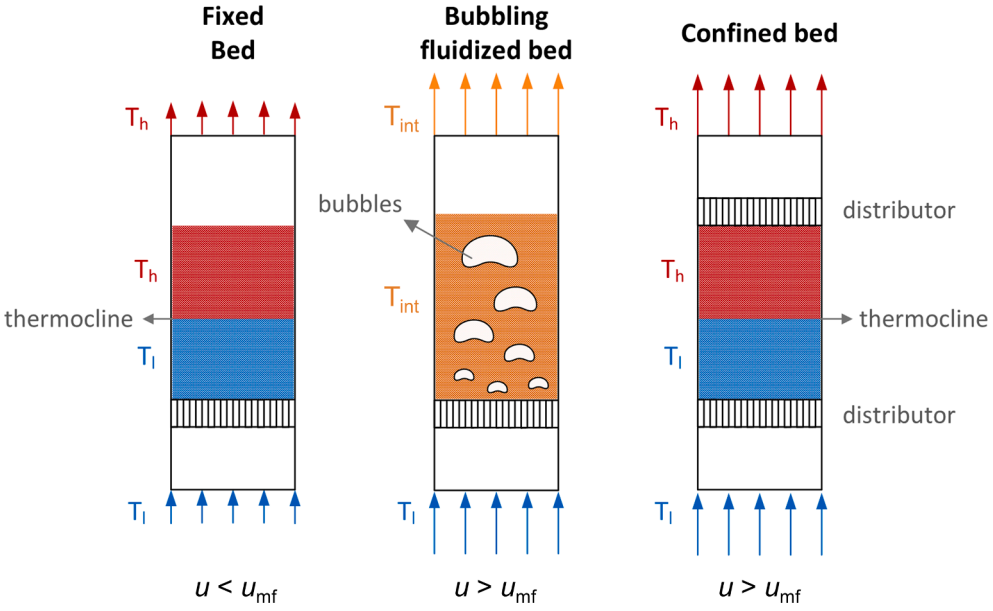

Fig. 3. Schematic view of the fixed, bubbling fluidized and confined beds operation during a discharge process of a granular material TES system.

Once the bed was charged, the fluidized bed heated the working fluid during the discharge process, when solar irradiation was not high enough. The TES system proposed here represents an alternative to the whole system proposed in Rovense et al. [30]. This TES system consists of a single tank where the granular material is confined with two fluid distributors to mechanically prevent fluidization, guaranteeing the operation of the system under a fixed bed regime, as stated in Section 3. The proposed TES system counts on several advantages: i) the subsystems required for the whole TES unit are reduced, ii) the operation under a fixed bed regime maximizes the exergy of the fluid at the outlet of the TES system / inlet of the turbine [17], and iii) the operation under fixed bed conditions prevent operational problems of fluidized beds, such as abrasion/erosion of tubes [44], attrition of particles [27], agglomeration formation [15], or de-fluidization of the bed [14].

The input data used for the thermo-economic optimization of the TES system based on confined granular material for the plant described in Rovense et al. [30] are reported in Table 3. The granular material proposed to fill the confined bed of the TES system for the case of study is regular silica sand with an average particle size of 750 μm and a typical value of the bed void fraction of 0.4 for the random packing of particles poured into the bed. The thermo-physical properties of silica sand used for the calculations are included in Table 4. The minimum fluidization velocity of these silica sand particles, estimated by the correlation of Carman-Kozeny [5] for the average bed temperature, i.e., for 630 °C, is $u_{mf} = 0.2$ m/s. The accuracy of the correlation of Carman-Kozeny to estimate u_{mf} at high temperature was proven by Soria-Verdugo et al. [33], comparing its predictions with experimental measurement for regular silica sand particles of similar particle size for a temperature range from room temperature to 600 °C.

5. Results and discussion

5.1. Thermal performance of the TES system

The inlet parameters of the case of study, reported in Table 3, were used to evaluate the evolution of the temperature in the confined bed of granular material representing the TES system. The confined bed was cylindrical in shape. For the characterization of the thermal performance of the TES system, the bed height was set arbitrarily to $H = 10$ m and the diameter D was varied to analyze the effect of the fluid velocity u on the thermocline thickness. Since a constant fluid mass flow rate of $\dot{m}_f = 50$ kg/s is kept constant, as indicated in Table 3, this results in a fluid velocity inversely proportional to the square of the bed diameter. For instance, considering a bed diameter of $D = 11.9$ m leads to an average fluid velocity of $u = 0.18$ m/s in the TES system. Calculating the fluid temperature as a function of time and bed height by means of Eq. (23), the discernment of the high and low temperature of the bed can be made as time progresses. This is illustrated in Fig. 4, where a contour plot of the fluid temperature as a function of time and bed height during the discharge process of the confined bed TES system is presented for an average fluid velocity of 0.18 m/s. In the figure, the fluid temperature along the bed height can be determined as a vertical line for specific values of time. For the discharge process, the entire bed is at high temperature at the beginning of the process, and the thermocline evolves from bottom to top of the confined bed as time progresses. The thermocline can be observed in Fig. 4 as the diagonal separating the high and low temperature zones of the bed. The increase of the thermocline thickness with time predicted by Eq. (27) can also be observed in the figure as a wider zone of intermediate temperatures for high values of the bed height and long times. The discharge time can be determined in the figure as the time for which the outlet temperature of the fluid coincides with the high temperature, i.e., drawing a horizontal line at the confined bed height, $H = 10$ m, until the temperature starts to decrease, obtaining a value of the discharge time slightly lower than 10 h for a fluid velocity of 0.18 m/s.

Table 3
Input data for the thermo-economic optimization of the TES system of the study case.

Parameter	Value
Fluid mass flow rate, $\dot{m}_f$ [kg/s]	50
Compressor pressure ratio, π_p [–]	6
Compressor polytropic efficiency, η_{p_c} [–]	0.915
Compressor isentropic efficiency, η_c [–]	0.894
Ambient temperature, T_a [K]	293
Ambient pressure, p_a [bar]	1
Turbine inlet pressure, p_i [bar]	5
Working fluid	Air (ideal gas)
TES high temperature, T_h [K]	1108
TES low temperature, T_l [K]	698
TES demand hours, t_i [h]	1 – 12

Table 4
Properties of the granular material used for the TES system of the study case.

Parameter	Value
TES granular material	Silica sand
Sand diameter, d_s [μm]	750
Bed porosity, ε [–]	0.4
Sand density, ρ_s [kg/m^3]	2600
Sand specific heat, c_{p_s} [J/kgK]	896
Sand thermal conductivity, k_s [W/mK]	1

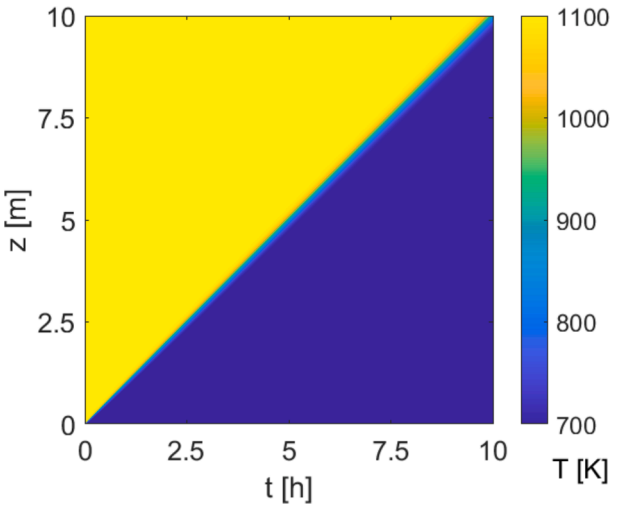

Fig. 4. Contour plot of the fluid temperature of the confined bed TES system for a fluid velocity of 0.18 m/s.

The local distribution of temperature in the confined bed for a specific instant can be determined by fixing the value of time in Eq. (23). Considering the walls of the TES system adiabatic as a first approximation, the discharge process would be one-dimensional, and the fluid and solids temperature would change only in the axial direction, i.e., the direction of the bed height, with no temperature variation in the radial direction. Fig. 5 a) represents the temperature distribution in the entire confined bed after 5 h of discharge process with a fluid velocity of 0.18 m/s. At that time, almost half of the bed is at the low temperature, while the half top of the confined bed remains at the high temperature. Thus, the thermocline is located around the middle of the bed, where a narrow zone with a temperature distribution from the high to the low temperature of the system, corresponding to the thermocline thickness, is visible in the figure. Considering the 1D discharge problem, Fig. 5 b) shows the temperature distribution along the bed height for $t = 5$ h and $u = 0.18$ m/s, where the sharp temperature change at around the middle of the confined bed height can be observed. The thermocline thickness can be determined in this figure as the region where temperature varies

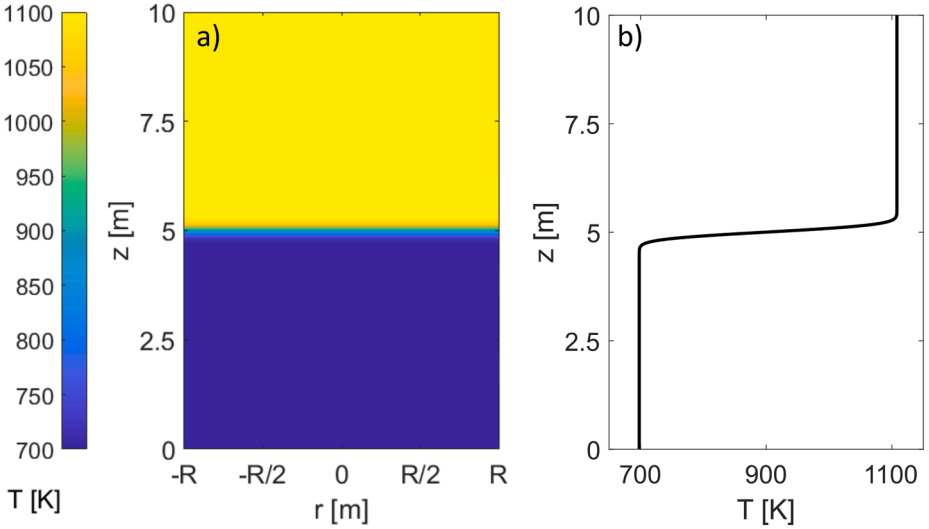

Fig. 5. Temperature distribution a) in the entire confined bed and b) along the confined bed height for a fluid velocity of 0.18 m/s after 5 h of the discharge process.

from the low to the high value with a deviation of 5 %, i.e., $\sigma = 0.05$ in Eq. (26), corresponding to $\delta_t = 0.61$ m for this case. Noticeably, the position of the thermocline is affected by the value of the porosity of the bed, as it has direct impact on the confined bed energy balance. However, as mentioned in Section 4, a standard value of a porosity of 0.4 is used in this work. It was observed that the thickness of the thermocline is not strongly affected by this parameter. Nevertheless, the sensitivity of the results to the value of the bed porosity is analyzed in Section 5.2.1.

The time evolution of the thermocline thickness in the confined bed can be determined by Eq. (27). The result is plotted in Fig. 6, where the growth of the thermocline thickness with time can be observed for various fluid velocities. In all cases, the thickness of thermocline increases with the square root of time, as a typical characteristic of a diffusion-controlled problem [35]. Fig. 6 shows that the thermocline thickness is proportional to the fluid velocity, obtaining high values of δ_t for greater values of u. Thus, low values of the fluid velocity are recommended to prevent an excessive growth of the thermocline, which would also contribute to limiting the pressure drop of the fluid circulating through the bed according to Eq. (32). However, an excessively low fluid velocity would result in a large bed diameter, leading to an overrun of the TES investment mainly due to the isolation material and the foundations of the confined bed TES system, as established by Eq. (37). Therefore, the optimization of the geometry and operating conditions of the confined bed TES system should be carried out considering both thermodynamic and economic factors.

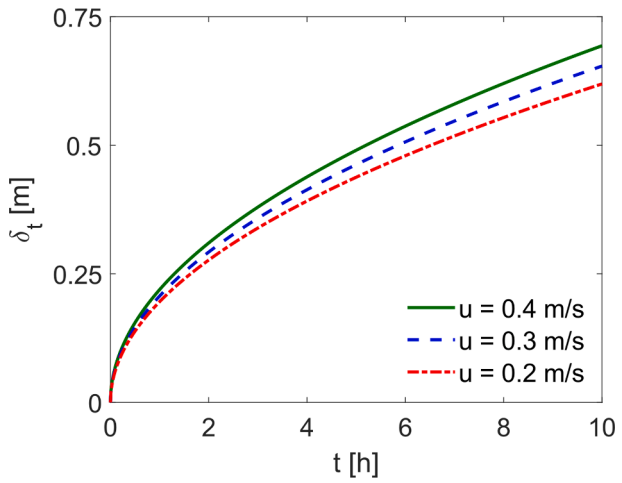

Fig. 6. Time evolution of the thermocline thickness for various fluid velocities.

5.2. Thermo-economic optimization of the confined bed TES system for the case of study

A confined bed TES system for the case of study presented in Section 4 was optimized considering thermodynamic and economic factors. The optimization was performed for a variable TES demand time, t_i, between 1 and 12 h, considering the operating conditions and thermophysical properties reported in Tables 3 and 4. First, the volume of the confined bed TES system, V, can be directly derived from the energy balance between the fluid and the solids as a function of the TES demand time:

$$V = \frac{\dot{m}_f c_{p_f} t_i}{\rho_s c_{p_s}(1-\varepsilon) + \rho_s c_{p_f} \varepsilon}. \tag{40}$$

Once the required volume of the confined bed is determined, V, the mass of solid particles, m_s, can be calculated as a function of the solids' density, ρ_s, and their void fraction, ε, as follows:

$$m_s = \rho_s (1-\varepsilon) V. \tag{41}$$

However, the volume of the confined cylindrical bed can be attained by multiple combinations of bed heights, H, and diameters, D. Each of these combinations result in a different average fluid velocity, u, for a fixed value of the mass flow rate of fluid of $\dot{m}_f = 50$ kg/s, as stated in Table 3 for the case of study. The average fluid velocity will affect the real discharge time of the system, t_d, calculated by solving Eq. (36), which will differ slightly from the TES demand time, t_i, because of the thickness of the thermocline. The geometry of the confined bed TES system can be optimized considering its effect on the exergy availability of the fluid at the outlet of the TES system, ΔE, Eq. (28), and on the total investment cost of the whole TES system, C, Eq. (37). The effect of the variable average fluid velocity, u, on the fluid exergy variation, ΔE, and the total investment cost, C, are represented in Fig. 7 for various TES demand times, t_i.

Fig. 7 a) shows the variation of the fluid exergy increment in the TES system during a discharge process as a function of the average fluid velocity. For all TES demand times, t_i, the curves of ΔE present a similar trend. Considering a constant fluid mass flow rate of $\dot{m}_f = 50$ kg/s, the fluid exergy increment in the TES system decreases with the average fluid velocities due to the increased pressure drop, as indicated in Eq. (42). The fluid exergy increment presents a maximum at low values of the average fluid velocity. A significant effect of the TES demand time, t_i, on the fluid exergy increase, ΔE, can also be observed in Fig. 7 a). This

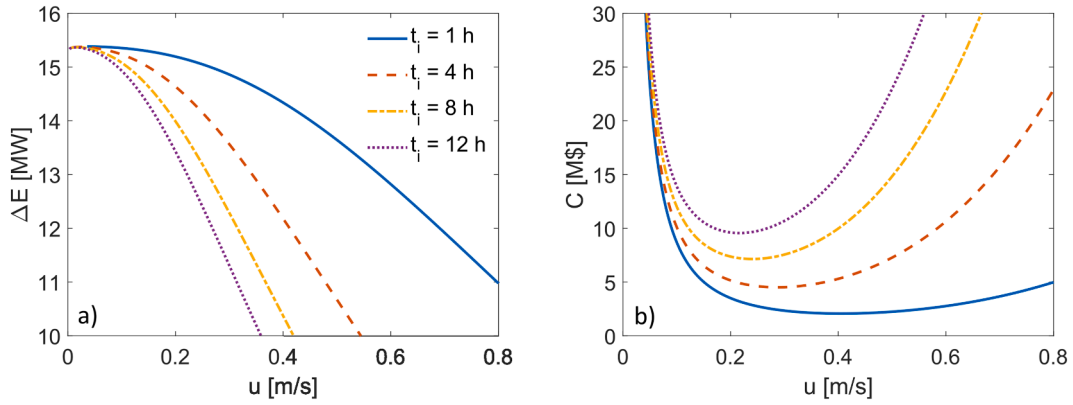

Fig. 7. Effect of the average fluid velocity on a) the fluid exergy increment and b) the total investment cost for various TES demand times.

effect is caused by the linear increase of the TES system volume with the demand time. Keeping a constant fluid mass flow rate, the same average fluid velocity can be only attained by maintaining the same bed diameter, D, and thus, to account for the volume increase for different TES demand times, a higher bed height, H, would be required for higher values of t_i. Therefore, a substantial increase of the TES system pressure drop, Eq. (42), is obtained for higher values of the demand time due to the greater bed height required, inducing a sharper reduction of the fluid exergy increment, ΔE, as the TES demand time, t_i, is increased.

The total investment cost of the TES system is shown in Fig. 7 b) as a function of the average fluid velocity for various values of the TES demand time. The shape of the curves is similar, with a sharp increase of the investment cost for low values of the average fluid velocity. This increase in the total investment cost is motivated by the cost of the TES vessel, i.e., the cost of stainless steel and the insulating materials. As stated above, the reduction of the average fluid velocity can be only attained by an increase of the bed diameter for a constant value of the fluid mass flow rate. Considering that the confined bed volume is constant for all average fluid velocities, with a different value for each demand time, the increase of D at low u causes a reduction of H. Thus, for low values of the average fluid velocity the bed will be shallow, with a low ratio H/D, resulting in an increased external surface of the confined bed which involves a vessel cost overrun. For intermediate values of the average fluid velocity, the total investment cost decreases fast to different values for each demand time due to the cost of the granular material, which is proportional to the bed volume (Table 2). Then, the total investment cost increases again for high values of the average fluid velocity due to the over cost of the compressor required to overcome the fluid pressure drop across the confined bed TES system. Therefore, the total investment cost of the TES system presents a minimum value for different average fluid velocities depending on the TES demand time, with higher costs for higher values of t_i due to the larger volume of the TES system.

The total investment cost per unit of fluid exergy increment was analyzed to optimize the average fluid velocity for each TES demand time. The results are depicted in Fig. 8. All curves present a high value of $C/\Delta E$ for low average fluid velocities as a result of the sharp increase of the total investment costs of the TES system and the decrease of the fluid exergy increment for low values of u. At high average fluid velocities, the ratio $C/\Delta E$ increases again because of the increasing pressure drop of the fluid circulating through the confined bed TES system, which motivates a reduction of the fluid exergy increment, ΔE, and an increase of total investment cost, C, as discussed above. Therefore, the total investment cost per unit of fluid exergy increment shows a minimum value for an optimal value of the average fluid velocity depending on the selected value of the TES demand time. The minimum value of the ratio $C/\Delta E$ increases for high values of the demand time because of the larger TES system required for higher demand times.

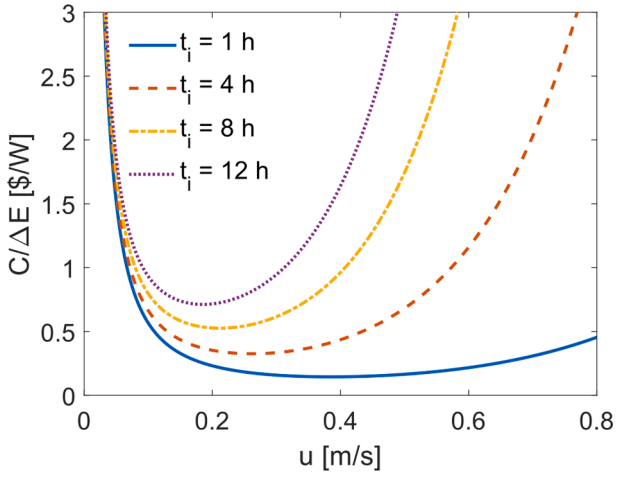

Fig. 8. Total investment cost per unit of fluid exergy increment.

The optimal average fluid velocity, defined as the velocity for which the ratio $C/\Delta E$ is minimum, and the minimum value of the ratio of investment cost to fluid exergy increment are plotted in Fig. 9 a) and b), respectively, as a function of the TES demand time. The optimal average fluid velocity decreases with the TES demand time because of the higher size required for the confined bed, which would lead to high fluid pressure drops for higher average fluid velocities. The values of the optimal average fluid velocity range from around 0.2 to 0.4 m/s, which, considering the estimation of the minimum fluidization velocity of the solids of 0.2 m/s, justifies the use of the confined bed to guarantee that the fixed bed regime is kept at fluid velocities above u_{mf} by mechanical confinement of the particles.

The minimum value of the total investment cost per unit of exergy increment of the fluid increases with the TES demand time, as anticipated in view of Fig. 8. However, the increases of the minimum value of $C/\Delta E$ with the TES demand time showed in Fig. 9 b) should be analyzed with caution. This parameter shows the investment cost per unit of fluid exergy increase, which is higher for increasing TES demand times. Nonetheless, a longer demand time involves a larger bed for which the discharge time is also longer. Thus, even though there is an increase of the investment cost per unit of fluid exergy increment for higher demand times, that increased fluid exergy can be maintained for a longer time, specifically during the whole discharge time, and then, the investment cost for high demand times should not be penalized without considering the effect of the discharge time.

To determine the discharge time of the confined bed TES system, the geometry of the bed and particularly the bed height is required. Once the optimal average fluid velocity of the bed is calculated for each demand

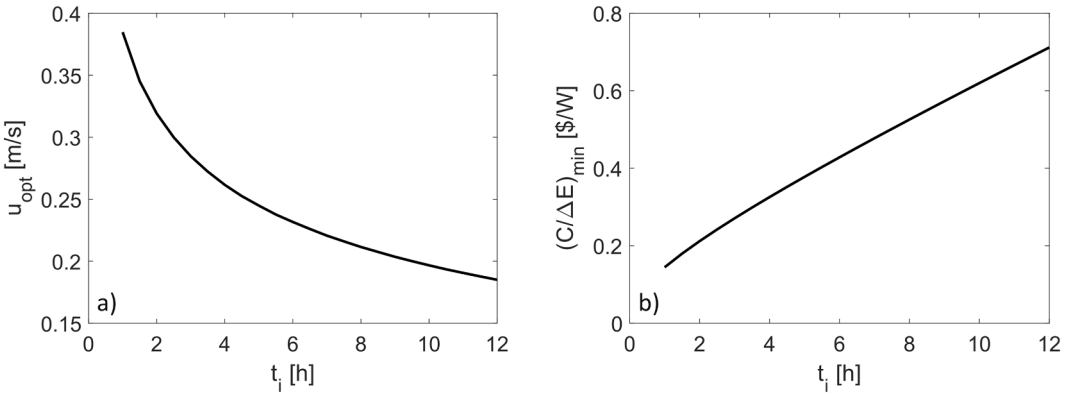

Fig. 9. a) Optimal average fluid velocity and b) minimum value of the investment cost per unit of fluid exergy increment.

time, the optimal bed diameter can be calculated from the constant fluid mass flow rate, and the optimal bed height from the volume of the TES system, which depends on the demand time. The results of the optimal diameter and height of the confined bed can be observed in Fig. 10. The optimal diameter of the bed increases slightly with the demand time, whereas a higher increase of the optimal bed height is observed. The increase of the optimal bed height together with the decrease of the optimal average fluid velocity with the demand time limit the value of the fluid pressure drop across the TES system. Considering the optimal values of the diameter and height of the confined bed for TES demand times ranging from 1 to 12 h, the aspect ratio of the cylindrical confined bed varies from 0.25 to 0.9 for the operating conditions of the case of study, shown in Table 3, and the selected characteristics of the solids, reported in Table 4. Additionally, once the optimal dimensions of the system were determined, the maximum temperature sustained by the different insulation materials proposed in Table 2 were evaluated, corroborating that each maximum temperature is lower than the maximum temperature allowed by the corresponding material.

Once the geometry and operating conditions of the confined bed TES system are established, the discharge time can be computed by solving Eq. (36) for the conditions corresponding to each TES demand time. The relation of the discharge time and the demand time is shown in Fig. 11 a), where a small effect of the thermocline can be observed as a slightly lower discharge time compared to the TES demand time. This low effect of the thermocline is motivated by the low values obtained for the optimal average fluid velocity, which lead to a thin thermocline, as shown in Fig. 5 and in the thermocline thickness equation, Eq. (27). A reduction of the demand time of around 2.4 % is obtained for the discharge time as an effect of the thermocline thickness. However, this effect could be much more significant for higher average fluid velocities and/or different particle sizes and properties. The discharge time was considered as the time for which the fluid exergy increment can be maintained for each case. Taking into account the discharge time, the evolution of the minimum investment cost per unit of fluid exergy increment times the discharge time is represented in Fig. 11 b) as a function of the TES demand time. Considering the linear increase of the actual discharge time with the demand time, $C/(\Delta E t_d)$ decreases when longer TES demand time are required. Therefore, according to Fig. 11 b), higher TES demand time results in a lower investment cost per unit of fluid exergy increment times discharge time. However, the TES demand time should be selected considering the solar multiple *SM* of the CSP plant and the higher operating cost derived from a longer discharge time.

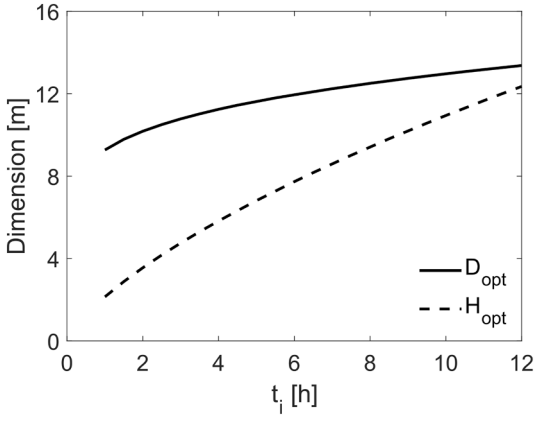

Fig. 10. Optimal dimensions of the confined bed TES system for the conditions stated in Tables 3 and 4.

5.2.1. *Sensitivity analysis*

The confined bed of the TES system designed for the case of study was optimized considering regular silica sand as granular material, with a particle size of 750 μm and a bed void fraction of 0.4. However, both the particle size of the solids conforming the bed, d_s, and the bed void fraction, ε, have a remarkable effect on the results of the optimization since the pressure drop of the fluid circulating along the packed bed depends strongly on the solids diameter and the bed void fraction, as can be seen in Eq. (33). Thus, to quantify the effect of the bed void fraction and the solids' diameter on the optimization of the confined bed, a sensitivity analysis of those parameters was performed.

Fig. 12 represents the effect of the bed void fraction on the optimal dimensions of the TES system for different demand times. Noticeably, varying the bed porosity within reasonable values, from 0.35 to 0.45, does not promote a qualitative change of the behavior of the TES system, however, it has implications on the optimal dimensions of the system, as shown in Fig. 12. The packing of the system has two different effects on the optimization process. On the one hand, a higher packing of the bed, i.e., a lower void fraction, implies a reduction of the volume required to fit a determined mass of solids, resulting in a more compact system. On the other hand, the void fraction strongly affects the pressure drop of the fluid in the bed, as shown in Eqs. (33) and (34). Thus, a higher packing of the bed, or lower void fraction, induces a significant increase of the pressure drop, which promotes a lower optimal velocity and/or bed height to limit the value of the pressure drop. The lower optimal velocity or bed height required for more densely packed beds is obtained by an increased value of the bed diameter, as depicted in Fig. 12. Therefore, reducing the void fraction of the bed results in a higher optimal diameter of the bed that enhances a reduction of the bed pressure drop by limiting the optimal velocity of operation and reducing the bed height. These tendencies of the optimal dimensions can be clearly observed in Fig. 12. All in all, the qualitative behavior of the system remains the same in all cases. However, the use of a confined bed is not consistent with loosely packed systems, provided that the mechanical confinement of the bed will forcedly promote the formation of a densely packed bed.

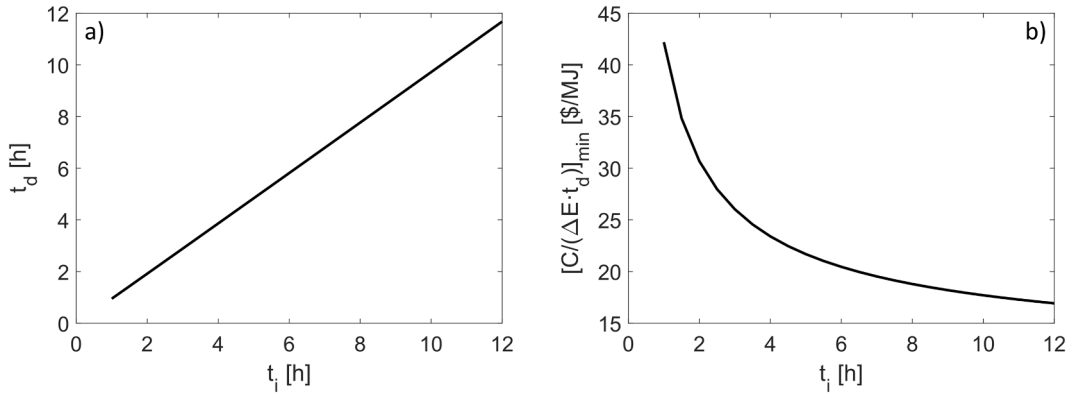

Fig. 11. a) Discharge time and b) minimum investment cost per unit of fluid exergy increment times discharge time.

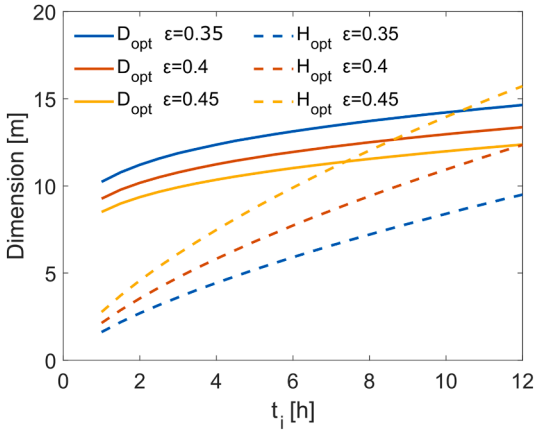

Fig. 12. Optimal dimensions of the confined bed TES system as a function of the bed void fraction.

To quantify the effect of the solids' diameter on the optimization of the confined bed, the operating parameters of the case of study (Table 3) and the thermo-physical properties of sand (Table 4) where used to optimize a confined bed conformed of silica sand particles of d_s ranging from 250 μm to 10 mm, for a fixed TES demand time of $t_i = 6$ h. The optimal dimensions of the cylindrical confined bed are represented in Fig. 13 as a function of the silica sand particle size. The significant reduction of the fluid pressure drop for higher granular material particle sizes results in much deeper optimal confined beds for coarser particles. The optimal bed height increases with the diameter of the solids, considerably faster for low values of d_s, for which small particle size increments lead to significant reductions of Δp. The aspect ratio of the optimal confined bed increases up to $H/D = 3.5$ for particle sizes of 10 mm. Nonetheless, the particle size of the solids conforming the confined bed of TES system should be selected low enough to avoid undesired temperature distributions inside single particles by keeping a low particle Biot number.

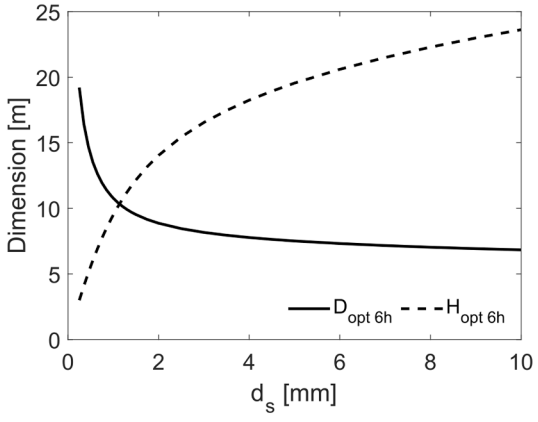

Fig. 13. Optimal dimensions of the confined bed TES system as a function of the diameter of the solid particles for a TES demand time of 6 h.

6. Conclusions

A new configuration using a confined bed is proposed as a granular material TES system to store sensible heat in a concentrated solar power plant. The selection of this novel confined bed is based on the idea of maximizing the exergy of the fluid leaving the TES system, which is coupled to the power block of the plant. An analysis of the performance of the thermocline in the confined bed during a discharge process was performed, quantifying the effect of the thickness of the thermocline on the discharge time. The effect of the thermocline on the discharge time was found to increase with the fluid velocity.

The effect of the thermocline was combined with a thermo-economic analysis of a confined bed TES system proposed for a case of study. This confined bed was optimized considering both thermodynamic and economic aspects. The optimal geometry and operating conditions of the confined bed were derived as a function of the demand time by minimizing the investment cost per unit of fluid exergy increment. The optimal fluid velocity for a confined bed of silica sand of 750 μm in diameter was found to be low, between 0.2 and 0.4 m/s, to prevent excessive increments of the fluid pressure drop across the confined bed, while the bed aspect ratio range between 0.25 and 0.9, depending on the TES demand time. However, the optimal fluid velocity is higher than the minimum fluidization velocity of the solids selected, thus, the novel concept of confined bed proposed is necessary to maximize the exergy availability of the fluid supplied to the turbine from the TES system. The optimal dimensions of the confined bed were found to depend strongly on the particle size of the granular material, since this parameter has a significant effect on the fluid pressure drop. Considering the effect of the thermocline thickness on the discharge time, the newly proposed confined bed TES system operates better for longer demand times, for which the total investment cost required to keep the fluid exergy increment during the discharge time is lower. However, the demand time of the TES system should be selected considering the solar multiple of the concentrated solar power plant to account for the excess of energy available to charge the TES system.

Declaration of Competing Interest

The authors declare that they have no known competing financial interests or personal relationships that could have appeared to influence the work reported in this paper.

Data availability

No data was used for the research described in the article.

Acknowledgments

This research was funded by the Spanish Government under the project STORESOL, reference number PID2019-109224RA-100. Eduardo Cano-Pleite also acknowledges support from the CONEX-Plus program funded by Universidad Carlos III de Madrid and the European Union's Horizon 2020 program under the Marie Sklodowska-Curie grant agreement No. 801538.

References

[1] J. Bell, A simple and pragmatic approximation to the normal cumulative probability distribution. Available at SSRN, 2015.
[2] A.M. Bonanos, E.V. Votyakov, Sensitivity analysis for thermocline thermal storage tank design, Renew. Energy 99 (2016) 764–771.
[3] A.M. Bonanos, E.V. Votyakov, Analysis of thermocline thermal energy storage systems with generic initial condition algebraic model, Sol. Energy 213 (2022) 154–162.
[4] R. Bayon, E. Rojas, Simulation of thermocline storage for solar thermal power plants: from dimensionless results to prototypes and real-size tanks, Int. J. Heat Mass Transf. 60 (2013) 713–721.
[5] P.C. Carman, Fluid flow through granular beds, Transactions of the Institution of Chemical Engineers 15 (1937) 150–166.
[6] F. Crespi, D. Sánchez, J.M. Rodríguez, G. Gavagnin, A thermo-economic methodology to select sCO_2 power cycles for CSP applications, Renew. Energy 147 (2020) 2905–2912.
[7] K. El Alami, M. Asbik, H. Agalit, Identification of natural rocks as storage materials in thermal energy storage (TES) system of concentrated solar power (CSP) plants - A review, Sol. Energy Mater. Sol. Cells 217 (2020), 110599.
[8] K.E. Elfeky, A.G. Mohammed, N. Ahmed, L. Lu, Q. Wang, Thermal and economic evaluation of phase change material volume fraction for thermocline tank used in concentrating solar power plants, Appl. Energy 267 (2020), 115054.
[9] S. Ergun, Fluid flow through packed columns, Chem. Eng. Prog. 48 (1952) 89–94.
[10] A.G. Fernández, J. Gomez-Vidal, E. Oró, A. Kruizenga, A. Solé, L.F. Cabeza, Mainstreaming commercial CSP systems: A technology review, Renew. Energy 140 (2019) 152–176.
[11] L.M. Garcia-Gutierrez, F. Hernández-Jiménez, E. Cano-Pleite, A. Soria-Verdugo, Experimental evaluation of the convection heat transfer coefficient of large particles moving freely in a fluidized bed reactor, Int. J. Heat Mass Transf. 153 (2020), 119612.
[12] P. Gauché , South African provisional patent application. 2014/03555, 2014.
[13] H. Ghaebi, M. Amidpour, S. Karimkashi, O. Rezayan, Energy, exergy and thermoeconomic analysis of a combined cooling, heating and power (CCHP) system with gas turbine prime mover, Int. J. Energy Res. 35 (2011) 697–709.
[14] J. Gómez-Hernández, A. Soria-Verdugo, J. Villa-Briongos, D. Santana, Fluidized bed with a rotating distributor operated under defluidization conditions, Chem. Eng. J. 195–196 (2012) 198–207.
[15] J. Gómez-Hernández, D. Serrano, A. Soria-Verdugo, S. Sánchez-Delgado, Agglomeration detection by pressure fluctuation analysis during Cynara cardunculus L. gasification in a fluidized bed, Chem. Eng. J. 284 (2016) 640–649.
[16] M. Hänchen, S. Brückner, A. Steinfeld, High-temperature thermal storage using a packed bed of rocks - Heat transfer analysis and experimental validation, Appl. Therm. Eng. 31 (2011) 1798–1806.
[17] F. Hernández-Jiménez, A. Soria-Verdugo, A. Acosta-Iborra, D. Santana, Exergy recovery from solar heated particles to supercritical CO_2, Appl. Therm. Eng. 146 (2019) 469–481.
[18] U. Herrmann, D.W. Kearney, Survey of thermal energy storage for parabolic trough power plants, J. Sol. Energy Eng. 124 (2002) 145–152.
[19] J.F. Hoffmann, T. Fasquelle, V. Goetz, X. Py, A thermocline thermal energy storage system with filler materials for concentrated solar power plants: Experimental data and numerical model sensitivity to different experimental tank scales, Appl. Therm. Eng. 100 (2016) 753–761.
[20] F.P. Incropera, D.P. de Witt, T.L. Bergman, A.S. Lavine, Fundamentals of Heat and Mass Transfer, sixth ed., John Wiley & Sons, United States of America, 2007.
[21] S.B.R. Karry, J. Werther, Gas distributor and plenum design in fluidized beds, in: W.-.-C. Yang (Ed.), Handbook of fluidization and fluid-particle systems, Marcer Dekker Inc, 2003, pp. 155–170.
[22] D. Kunii, O. Levenspiel, Fluidization Engineering, second ed., Butterworth Heinemann, Boston, 1991.
[23] S. Kuravi, J. Trahan, D.Y. Goswami, M.M. Rahman, E.K. Stefanakos, Thermal energy storage technologies and systems for concentrating solar power plants, Prog. Energy Combust. Sci. 39 (2013) 285–319.
[24] W. Lou, Y. Fan, L. Luo, Single-tank thermal energy storage systems for concentrated solar power: Flow distribution optimization for thermocline evolution management, J. Storage Mater. 32 (2020), 101749.
[25] J. Marti, L. Geissbühler, V. Becattini, A. Haselbacher, A. Steinfeld, Constrained multi-objective optimization of thermocline packed-bed thermal-energy storage, Appl. Energy 216 (2018) 694–708.
[26] A. Meier, W.D. Winkler, Experiment for modelling high temperature rock bed storage, Solar Energy Materials 24 (1991) 255–264.
[27] M. Miao, X. Yao, S. Zhang, X. Jiang, S. Ren, H. Yang, M. Zhang, Attrition performance and morphology of limestone under different conditions in fluidized bed, Fuel Process. Technol. 221 (2021), 106939.
[28] A. Morato-Godino, S. Sánchez-Delgado, N. García-Hernando, A. Soria-Verdugo, Pyrolysis of Cynara cardunculus L. samples - Effect of operating conditions and bed stage on the evolution of the conversion, Chem. Eng. J. 351 (2018) 371–381.
[30] F. Rovense, M.A. Reyes-Belmonte, J. González-Aguilar, M. Amelio, S. Bova, M. Romero, Flexible electricity dispatch for CSP plant using un-fired closed air Brayton cycle with particles based thermal energy storage system, Energy 173 (2019) 971–984.
[31] D. Schlipf, E. Faust, G. Schneider, H. Maier, First operational results of a high temperature energy storage with packed bed and integration potential in CSP plants, AIP Conference Proceedings, DOI 10 (1063/1) (2017) 4984445.
[32] K. Skrbek, V. Bartunèk, D. Sedmidubský, Molten salt-based nanocomposites for thermal energy storage: Materials, preparation techniques and properties, Renew. Sustain. Energy Rev. 164 (2022), 112548.
[33] A. Soria-Verdugo, A. Morato-Godino, L.M. García-Gutiérrez, N. García-Hernando, Pyrolysis of sewage sludge in a fixed and bubbling fluidized bed – Estimation and experimental validation of the pyrolysis time, Energ. Conver. Manage. 144 (2017) 235–242.
[34] A. Soria-Verdugo, E. Cano-Pleite, A. Panahi, A.F. Ghoniem, Partitioning of a wide bubbling fluidized bed with vertical internals to improve local mixing and bed material circulation, Powder Technol. 408 (2022), 117771.
[35] W.P. Sun, M. Militzer, J.J. Jonas, Diffusion-controlled growth and coarsening of MnS during hot deformation, Metall. Trans. 23A (1992) 3013–3023.
[36] S. Trevisan, R. Guédez, B. Laumert, Thermo-economic optimization of an air driven supercritical CO2 Brayton power cycle for concentrating solar power plant with packed bed thermal energy storage, Sol. Energy 211 (2020) 1373–1391.
[37] S. Trevisan, Y. Jemmal, R. Guedez, B. Laumert, Packed bed thermal energy storage: A novel design methodology including quasi-dynamic boundary conditions and techno-economic optimization, J. Storage Mater. 36 (2021), 102441.
[38] S. Trevisan, W. Wang, R. Guedez, B. Laumert, Experimental evaluation of an innovative radial-flow high-temperature packed bed thermal energy storage, Appl. Energy 311 (2022), 118672.
[39] K. Vignarooban, X. Xu, A. Arvay, K. Hsu, A.M. Kannan, Heat transfer fluids for concentrating solar power systems – a review, Appl. Energy 146 (2015) 383–396.
[40] E. Votyakov, A. Bonanos, A perturbation model for stratified thermal energy storage tanks, Int. J. Heat Mass Transf. 75 (2014) 218–223.
[41] E.V. Votyakov, A.M. Bonanos, Algebraic model for thermocline thermal storage tank with filler material, Sol. Energy 122 (2015) 1154–1157.
[42] N. Wakao, S. Kaguei, T. Funazkri, Effect of fluid dispersion coefficients on particle-to-fluid heat transfer coefficients in packed beds: correlation of Nusselt numbers, Chem. Eng. Sci. 34 (3) (1979) 325–336.
[43] J. Weiss, I. Ortega-Fernández, R. Müller, D. Bielsa, T. Fluri, Improved thermocline initialization through optimized inlet design for single-tank thermal energy storage systems, J. Storage Mater. 42 (2021), 103088.
[44] L. Xu, K. Luo, Y. Zhao, J. Fan, K. Cen, Multiscale investigation of tube erosion in fluidized bed based on CFD-DEM simulation, Chem. Eng. Sci. 183 (2018) 60–74.
[45] Z. Yang, S. Garimella, Thermal analysis of solar thermal energy storage in a molten-salt thermocline, Sol. Energy 84 (2010) 974–985.
[46] G. Zanganeh, A. Pedretti, S. Zavattoni, M. Barbato, A. Steinfeld, Packed-bed thermal storage for concentrated solar power - Pilot-scale demonstration and industrial-scale design, Sol. Energy 86 (10) (2012) 3084–3098.
[47] Y. Zhu, D. Wang, P. Li, Y. Yuan, H. Tan, Optimization of exergy efficiency of a cascaded packed bed containing variable diameter particles, Appl. Therm. Eng. 188 (2021), 116680.